

This document is confidential and is proprietary to the American Chemical Society and its authors. Do not copy or disclose without written permission. If you have received this item in error, notify the sender and delete all copies.

Silicon Nanowire Sensors Enable Diagnosis of Patients *via* Exhaled Breath

Journal:	ACS Nano
Manuscript ID	nn-2016-03127b.R4
Manuscript Type:	Article
Date Submitted by the Author:	n/a
Complete List of Authors:	Shehada, Nisreen; Technion Israel Institute of Technology, Chemical Engineering Cancilla, John ; Complutense University of Madrid, Chemical Engineering Torrecilla, José; Universidad Complutense de Madrid, Chemical Engineering Pariente, Enrique ; Complutense University of Madrid, Department of Chemical Engineering Brönstrup, Gerald ; Max-Planck-Institute for the Science of Light Christiansen, Silke; Max-Planck-Institute for the Science of Light Johnson, Douglas ; Baptist Cancer Institute Leja, Marcis; University of Latvia, Faculty of Medicine Davies, Michael; Liverpool University, Molecular & Clinical Cancer Medicine Liran, Ori; Sheba Medical Center at Tel Hashomer Peled, Nir; Sheba Medical Center at Tel Hashomer Haick, Hossam; Technion - Israel Institute of Technology, Department of Chemical Engineering

SCHOLARONE™
Manuscripts

Silicon Nanowire Sensors Enable Diagnosis of Patients via Exhaled Breath

Nisreen Shehada⁽¹⁾, John C. Cancilla⁽²⁾, Jose S. Torrecilla⁽²⁾, Enrique S. Pariente⁽²⁾, Gerald Brönstrup⁽³⁾, Silke Christiansen⁽³⁾, Douglas W. Johnson⁽⁴⁾, Marcis Leja⁽⁵⁻⁷⁾, Michael P. A. Davies⁽⁸⁾, Ori Liran⁽⁹⁾, Nir Peled⁽⁹⁾, and Hossam Haick^{*(1)}

⁽¹⁾ Department of Chemical Engineering and Russell Berrie Nanotechnology Institute, Technion – Israel Institute of Technology, Haifa 3200003, Israel.

⁽²⁾ Department of Chemical Engineering, Complutense University of Madrid, Madrid 28040, Spain.

⁽³⁾ Max-Planck-Institute for the Science of Light, Günther-Scharowsky-Strasse 1, Erlangen 91058, Germany.

⁽⁴⁾ Florida Radiation Oncology Group, Department of Radiation Oncology, Baptist Cancer Institute (BCI), 1235 San Marco Boulevard., Suite 100, Jacksonville, FL 32207, US.

⁽⁵⁾ Faculty of Medicine, University of Latvia, 19 Raiņa boulv., LV1586, Riga, Latvia

⁽⁶⁾ Department of Research, Riga East University Hospital, 6 Linezera iela, Riga, Latvia, LV1006

⁽⁷⁾ Digestive Diseases Centre GASTRO, Riga, Latvia. 6 Linezera iela, Riga, Latvia, LV1006

⁽⁸⁾ Molecular & Clinical Cancer Medicine, University of Liverpool, Apex Building, 6 West Derby Street, Liverpool, L7 8TX, United Kingdom.

⁽⁹⁾ Thoracic Cancer Research and Detection Center, Sheba Medical Center, Tel Hashomer and Tel-Aviv University, Tel Aviv, Israel.

Keywords: nanowire; sensor; disease; cancer; diagnosis; breath; volatile organic compound

Abstract:

Two of the biggest challenges in medicine today are the need to detect diseases in a non-invasive manner, and to differentiate between patients using a single diagnostic tool. The current study targets these two challenges by developing a molecularly-modified Silicon Nanowire Field Effect Transistors (SiNW FETs) and showing its use in the detection and classification of many disease breathprints (lung cancer, gastric cancer, asthma and Chronic Obstructive Pulmonary Disease). The fabricated SiNW FETs are characterized and optimized based on a training set that correlated their sensitivity and selectivity towards volatile organic compounds (VOCs) linked with diseased states. The best sensors obtained in the training set are then examined under real-world clinical conditions, using breath samples from 374 subjects. Analysis of the clinical samples showed that the optimized SiNW FETs can detect and discriminate between almost all binary comparisons of the diseases under examination with >80% accuracy. Overall, this approach has the potential to support detection of many diseases in a direct positive way, which can reassure patients and prevent numerous negative investigations.

1
2
3 Physicians are always challenged by the need to give the correct diagnosis as early
4 in the onset of a disease is possible, whether the disease-related symptoms are
5 absent or not evident.¹ Symptoms are not always characteristic of one particular
6 disease; overlap of symptoms is common in, for example, lung diseases.² Patients
7 with different respiratory diseases, such as malignant or benign tumors, or
8 substantially less severe diseases, may have similar symptoms, e.g. cough, chest
9 pain, difficulty to breathe, etc. These symptoms may be characteristic of lung cancer
10 (LC), pneumonia, asthma, and chronic obstructive pulmonary disease (COPD).^{1,2}
11 Therefore, it is of particular clinical importance to find a diagnostic tool capable of
12 distinguishing between these diseases. A diagnostic tool that involves no needle,
13 surgery and/or active materials and/or radioactive exposure would have a benefit.
14
15
16
17
18
19

20 A highly promising approach that could meet the aforementioned need is
21 based on the detection and classification of the disease breathprint, viz. the chemical
22 profiles of highly- and semi-VOCs in exhaled breath linked with disease.³⁻¹⁵ The
23 rationale behind this approach relies on the fact that VOCs generated by cellular
24 metabolic pathways during a specific disease circulate in the blood stream and
25 diffuse into exhaled breath, which is easily sampled.^{4,16,17} In certain instances,
26 analysis of breathprints offers several potential advantages, such as: (a) breath
27 samples are non-invasive and easy to obtain; (b) breath contains less complicated
28 mixtures than either serum or urine; and (c) breath testing has the potential for direct
29 and real-time diagnosis and monitoring.^{3,18-21}
30
31
32
33
34

35 Several mass-spectrometry and spectroscopy studies have shown that the
36 breathprint of a specific disease differs from that of healthy controls.²²⁻²⁶ Some of the
37 investigated VOCs are present in different concentrations in the breath of patients
38 with a specific disease than in the breath of controls.²²⁻²⁶ Spectrometry and
39 spectroscopy techniques are powerful tools for detecting VOC of breathprints.
40 However, to date, these techniques has been impeded by the need for expensive
41 equipment, high levels of expertise to operate such instruments, the speed required
42 for sampling and analysis, and the need for pre-concentration techniques.^{22,27-29} For
43 breathprint testing to become a clinical reality, several advances in the sensor
44 development are needed. Chemical sensor matrices, based on nanomaterials, are
45 more likely to become clinical and laboratory diagnostic tools, because they are
46 significantly smaller, easier-to-use, and less expensive.^{18,30,31} An ideal chemical
47 sensor for breathprint analysis should be sensitive at very low VOC concentrations in
48 the presence of water vapor because headspace of clinical samples is fully
49 humidified. Furthermore, it should respond rapidly and differently to small changes in
50 concentration, and provide a consistent output specific to a given exposure.^{18,30,31}
51
52
53
54
55
56
57
58
59
60

1
2
3 When not in contact with the analyte, the sensor should return to its baseline state
4 rapidly, or be simple and inexpensive so that one could manufacture large numbers
5 of disposable units.
6

7 We have developed Silicon Nanowire Field Effect Transistors (SiNW FETs)³²⁻⁴⁴
8 as the sensing matrices for the detection and discrimination between disease
9 breathprints. As representative diseases, we chose gastric cancer (**GC**), lung cancer
10 (**LC**), asthma and Chronic Obstructive Pulmonary Disease (**COPD**). **NOTE:** For this
11 study, the asthma and COPD are considered as a control group for LC, and is
12 abbreviated as “**AC**” henceforth. These diseases cover both the direct and quasi-
13 direct track to the breath.^{4,16} Indeed, GC-related VOCs might reach the breath directly
14 through the esophagus or from the lung alveoli. While LC- and AC-related VOCs
15 reach the breath either by release directly into the airways or by diffusion in alveoli.
16 The SiNW FETs are characterized and optimized based on a training set that
17 correlated their sensitivity and selectivity towards the VOCs linked with the disease
18 states under examination. The best sensors obtained in the training set are examined
19 under real-world clinical conditions, using breath samples from 374 subjects. The
20 high sensitivity, low-power consumption, fast-response times, and the compatibility
21 with conventional silicon technology and readout circuitry, have the potential to get
22 SiNW FETs to give us simple signal transductions of disease breathprints, as well as
23 being amenable to miniaturization and scalability.⁴⁵⁻⁵⁰
24
25
26
27
28
29
30
31
32
33
34
35
36

37 **Results and Discussion**

38 **Preparation of molecularly-modified SiNW FETs**

39 The study consisted of 3 phases (**Figure 1a**). In the first, FETs based on well-aligned
40 array of SiNWs (density ~ 1 NW/ $100 \mu\text{m}^2$; 40 ± 8 nm in diameter; and $8.5 \pm 1.5 \mu\text{m}$
41 in length) were fabricated and characterized. Each SiNW FET was coated with different
42 molecular modification (**Table 1**). The aim of the molecular modification was to
43 passivate the surface states on the SiNW and optimize the interaction of VOCs with
44 the SiNWs. Four SiNW FETs were coated with molecules having mostly non-polar
45 (functional) side-groups (S1-S3 & S5) to improve their interaction with the non-polar
46 VOCs in the breathprint. Two SiNW FETs were coated with molecules having mostly
47 polar side groups (S4 & S6) to improve their interaction with the polar VOCs found in
48 the breathprint.
49
50
51
52
53
54
55
56
57
58
59
60

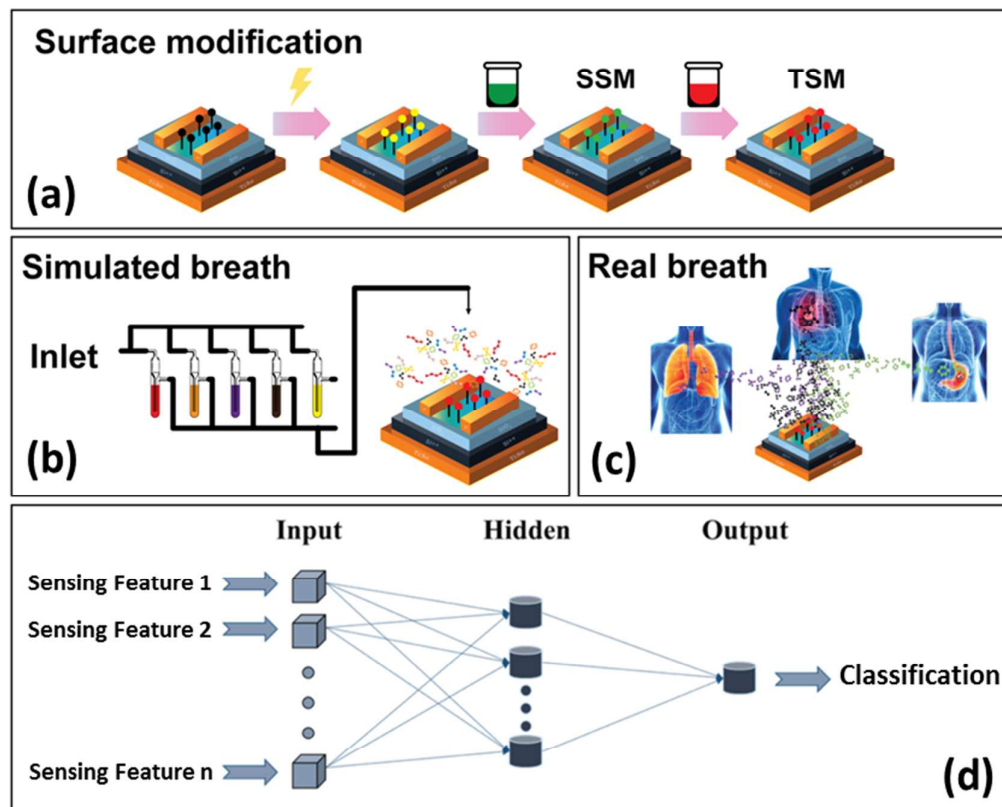
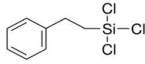
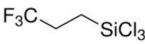
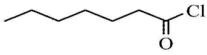
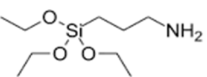
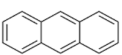
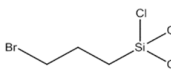


Figure 1. Schematic representation of the experimental procedure divided into: **(a)** surface modification of the SiNW FET sensors (SSM: single-step modification; TSM: 2-step modification); **(b)** exposure of sensors to breathprint simulants, representative VOCs recognized as potential biomarkers of each disease; and **(c)** exposure to real breath samples of patients suffering from known diseases, compared with healthy control volunteers. **(d)** Representation of the artificial neural networks (ANN)^{33,51} analysis method, where the sensing features are the inputs of the model, and the sample classification label is the output. ANNs are machine-learning algorithms that use a set of input vectors (sensing features in **Figure 1b**) to determine weighted parameters and mathematical functions, and to classify the samples (the sample classification label is the output).

Table 1: List of the molecular modifications used to coat the SiNWs - to optimize the interaction of the SiNW FETs with the breathprint-related VOCs

Sensor #	Modification	Structure
S1	Trichloro phenethyl silane (TPS)	
S2	Trichloro trifluoro propyl silane (TTPS)	
S3	Heptanoyl Chloride	
S4	3-Aminopropyl triethoxysilane (APTES)	
S5	Anthracene	
S6	Bromopropyl trichlorosilane (BPTS)	

Testing the sensors exposed to simulants of disease breathprints

In the second phase of the study, the molecularly-modified SiNW FET sensors were exposed to a number of VOCs presumed as breathprint biomarkers for the chosen diseases: GC, LC and AC (**Table 2**). The presumed VOCs linked with GC conditions *via* breathprint are: 2-propenenitrile, furfural, 6-methyl-5-hepten-2-one.^{14,31} The presumed VOC linked with AC conditions by breathprint is pentane.³¹ The presumed VOCs linked with LC conditions by breathprint are: heptane, decane, 2-methylpentane, 2-ethyl-1-hexanol, propanal, pentanal and acetone.³¹ Each SiNW FET was exposed to 4 concentrations of each VOC, and each exposure was repeated 3 times. In each exposure to VOC, the source-drain current (I_{ds}) vs. back gate voltage (V_{gs}) characteristic curve was obtained by sweeping the gate voltage between +40V and -40V (**Figure 2a**). For the sake of reference, I_{ds} - V_{gs} curves were obtained in vacuum before and after exposure to the VOC (**Figure 2a**).

Table 2: List of the representative VOCs linked with gastric cancer (GC), asthma & COPD (AC), or lung cancer (LC) from breathprint showing significant statistical differences ($p < 0.05$ in previous clinical studies). The VOC concentrations exposed to the molecularly-modified SiNW FETs, as well as the transition from concentration in p_a/p_o terms (p_a is the partial pressure of the VOC and p_o is the vapor pressure of the VOC) to parts per billion units (ppb), are presented.

Disease	VOC	P_a (mmHg)	Concentrations tested (p_a/p_o)	Concentrations tested (ppb)
GC	2-Propenenitril	83	0.001-0.008	100-870
	Furfural	2	0.001-0.008	2.6-21
	6-Methyl-5-heptene-2-one	0.8	0.001-0.008	0.98-7.9
AC	Pentane	6.2	0.001-0.008	8-65
LC	Heptane	40	0.001-0.008	50-420
	Decane	1.5	0.001-0.008	2-15
	2-Methylpentane	350.3	0.001-0.008	460-3680
	2-Ethyl-1-hexanol	0.23	0.001-0.008	0.29-2.36
	Propanal	258	0.0005-0.004	170-1360
	Pentanal	26	0.001-0.008	34-273
	Acetone	230	0.001-0.008	300-2420

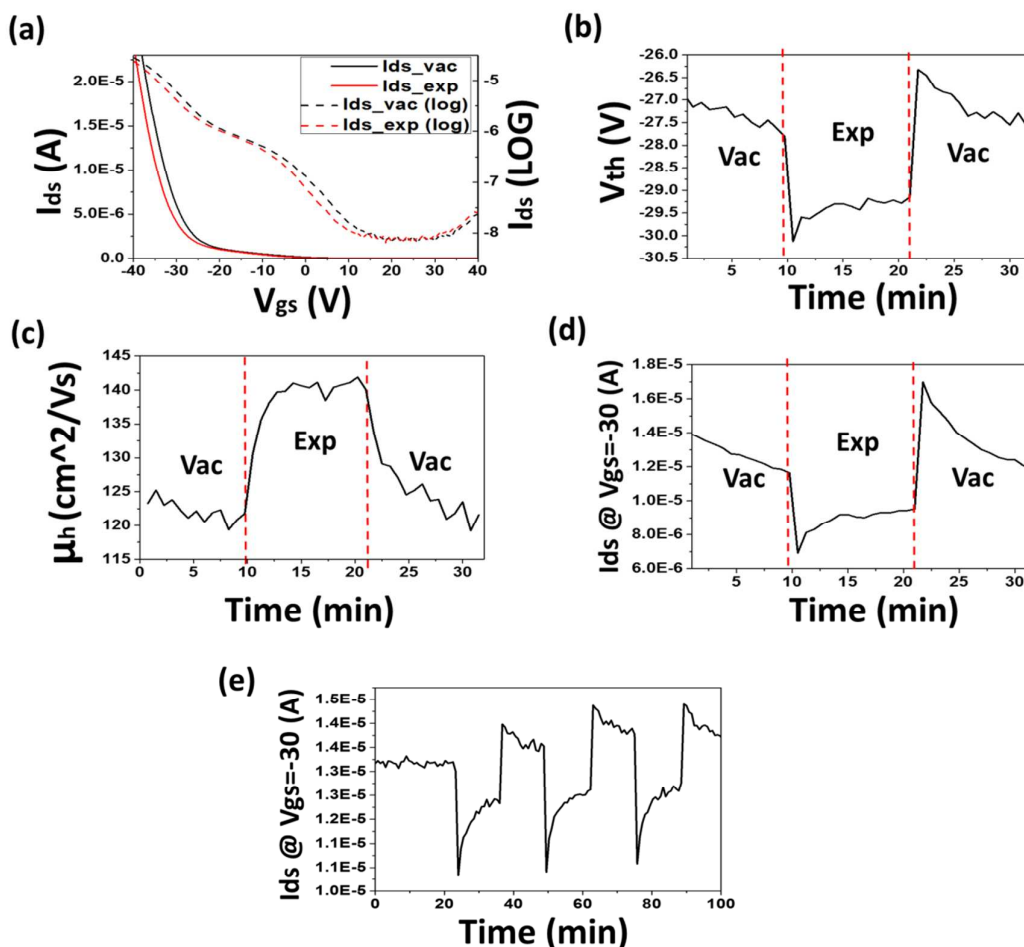


Figure 2. (a) Characteristic I_{ds} - V_{gs} curve of SiNW FET modified with heptanoyl chloride (S3) in vacuum (black line) and on exposure to 2-propenenitrile at a concentration of $p_a/p_0=0.001$ (red line). Curves are presented in both linear (solid line) and logarithmic (dashed line) scales. Sensing response of: (b) V_{th} , (c) μ_h and (d) I_{ds} @ $V_{gs} = -30$ V on exposure to 2-propenenitrile at a concentration of $p_a/p_0=0.001$. “Vac” stands for “vacuum” and “Exp” stands for exposure. (e) 3 repetitive response cycles of I_{ds} @ $V_{gs} = -30$ V exposed to 2-propenenitrile ($p_a/p_0=0.001$) condition for evaluating the repeatability of the sensing signals.

In most instances, exposing the SiNW FETs to VOCs resulted in a change in the I_{ds} - V_{gs} curves. **Figure 2a** presents the characteristic I_{ds} - V_{gs} curve of a SiNW FET modified with heptanoyl chloride (S3) under vacuum (black lines) and under exposure to $p_a/p_0=0.001$ of 2-propenenitrile (red lines). The FET curve changes on exposure to 2-propenenitrile. Closer examination of the curves shows that several FET features are changed on exposure, which include the voltage threshold (V_{th} ; the voltage under which the charge transfer regime changes from depletion to accumulation), the charge carrier (hole) mobility (μ_h ; the velocity of the charge

1
2
3 carriers moving under the influence of the electrical field), and the I_{ds} @ different V_{gs}
4 values. The extraction and calculation of these features is described in the
5 Experimental Methods section. As these features change with exposure, their values
6 (which can be monitored and recorded during the experiment) may be informative.
7 For example, the V_{th} values decrease on exposure to 2-propenenitrile from -27 to
8 -29.5V (**Figure 2b**) at the time the μ_h values increase from 125 to 140 $\text{cm}^2/\text{V}\cdot\text{s}$
9 (**Figure 2c**), and the I_{ds} @ $V_{gs}=-30\text{V}$ values decrease slightly from 120 to 80 μA
10 (**Figure 2d**). In the representative example (**Figure 2e**), repeated exposure cycles on
11 the same sensor are usually characterized by a relatively stable baseline and an
12 almost repeatable sensing features from cycle to cycle ($\pm 3\%$ variance).
13
14
15
16
17

18 The detection limit of the sensors to each VOC as well as the concentrations
19 found in breath can be found in the Supporting Information (**Table S1**). The detection
20 limit of each sensor is different and depends on the VOC's structure. In this context, it
21 is important to clarify that the SiNW FET sensors do not obey the lock-and-key
22 sensing approach.^{18,31} Instead, they have affinity to multiple VOCs and, therefore, the
23 sensing signal on exposure to a mixture of VOCs (e.g., a breath sample) reflects the
24 fingerprint of *all* the VOCs in it. Under these circumstances, different molecular
25 modifications of the SiNW change the affinity balance between the different VOCs
26 found in a specific mixture. Therefore, even if the detection limit of specific SiNW FET
27 to a certain VOC is higher than its concentration in the breath, the SiNW FET can still
28 detect the change in breath sample composition, as the overall change (sum) of VOC
29 changes in the breath due to disease state is in the range of a few to 10s of ppm.
30 These SiNW FETs have a very wide dynamic range between their limit of detection
31 (Table 1) up to thousands of ppm, when a thin film of condensed liquid begins to
32 develop on the surface of the sensors.
33
34
35
36
37
38
39
40

41 The ability to separate disease-related VOCs by a single sensor stems from
42 their ability to respond simultaneously to different VOCs, each of which induces a
43 different effect on the FET features due to one or a combination of the following
44 scenarios: **(i)** charge-charge interactions between the functional group of the
45 modified SiNW, which changes the charge density on the surface of the SiNW,
46 resulting in a change to V_{th} , μ_h or the currents in the linear region; **(ii)** addition of polar
47 or polarizable molecules on the surface of the SiNW, which changes the electrical
48 field on the surface, resulting in a change to the value of the subthreshold currents
49 and other features, similarly to molecular gating phenomena previously reported,³⁵
50 **(iii)** passivation of the surface states by the VOCs.^{34,35}
51
52
53
54
55

56 Investigation of the change in the entire $I_{ds}-V_{gs}$, mainly the depletion and
57 accumulation features, could help significantly an increase in the number of multiple
58
59
60

sensing features. These features operate as “virtual sensors”, viz. a set of independent sensing signals extracted from the electrical measurements of the device, and can be monitored separately as if they are individual sensors. This behavior leads to a decrease in the number of sensors needed for classification, and thus simplifies the system in terms of its supporting circuitry and infrastructure. To avoid unnecessary computation, a process of feature selection was applied by choosing only features with a signal-to-noise ratio >3 and by choosing only features that represent physical phenomena in the device.

Following the initial feature selection, artificial neural network (ANN) analysis was applied. Its purpose was to test the ability of the sensors to correlate VOCs with the disease to which they should relate, and to assess which sensor would be more suitable for disease diagnosis. ANN was applied on the basis of 36 samples for GC simulation, 12 samples for AC simulation, and 84 samples for LC simulation. Separation of GC-related VOCs from AC biomarkers was called “**Test-A**”; separation of LC-related VOCs from AC-related VOCs was **Test-B**; and separation between LC- and GC-related VOCs was “**Test-C**”. In **Test-A** and **Test-B**, the cancer group was considered the “positive” group, whereas AC was considered the “negative” group. In **Test-C**, LC was considered the “positive” group and GC was considered “negative”. The success in classification of the ANN analysis in each test is presented in **Figure 3**.

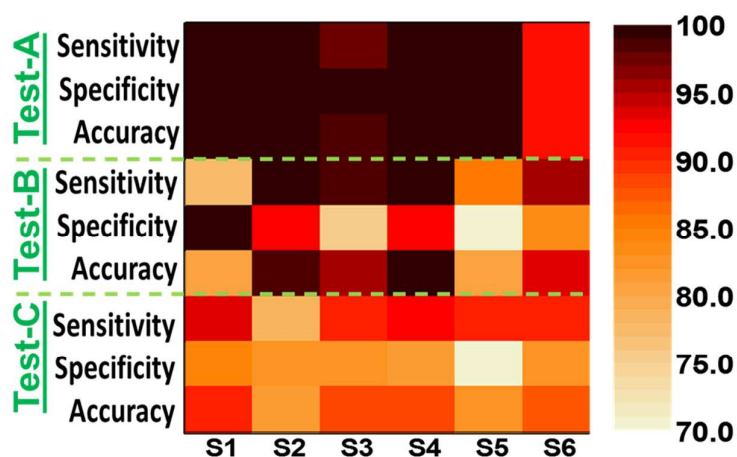


Figure 3. Classification results of sensing signals obtained from the molecularly-modified SiNW FETs upon exposure to a simulated VOC-related breathprint of the diseases. The color bar indicates the percentage of correct classification of samples comparing VOC of GC vs AC (Test-A); LC vs AC (Test-B); and LC vs GC (Test-C).

1
2
3 The ANN model calculated values of sensitivity, specificity and accuracy of
4 each comparison, the method being found in the Experimental Methods section.
5 Results from the vast majority of the sensors (**Figure 3**), and in most comparisons,
6 were satisfactory (>80% accuracy). Besides this accuracy for the classification, a few
7 important findings were recorded. In **Test-A**, most sensors correctly classified 100%
8 of the cases, irrespective of the vapor pressure values of the VOCs. In **Test-B**, S4
9 had a similar classification ability to S2 and S3 for LC (~100% accuracy) and gave
10 slightly better classification than S1, S5 and S6. On the other hand, S1 showed the
11 highest classification ability of AC samples (100%). In **Test-C**, S1 again gave the
12 highest percentage of correct classification; 93% for LC-related VOCs and 85% for
13 GC-related VOCs, resulting in 92% accuracy.
14
15
16
17
18
19
20

21 **Validation of the sensors in a clinical study**

22 To validate the performance of the SiNW FETs under lab conditions using simulants
23 of breathprint-related VOCs, clinical trials were carried out with the same sensors
24 (Experimental Methods section); the design of the clinical study is shown in **Figure 4**.
25 Briefly, breath samples were collected from 374 volunteers belonging to 4 groups:
26 control subjects not suffering from any of the conditions tested (n=129), LC patients
27 (n=149), GC patients (n=40) and AC patients (n=56). Cancer patients were also
28 divided into 2 groups according to the staging of the cancer: early (stages 1 and 2)
29 and advanced (stages 3 and 4). Additional information was also collected from the
30 volunteers, including age, gender, smoking status, *etc.*, shown in **Figure 4b**. Clinical
31 studies provides 3 main advantages over the simulated breathprint studies, because
32 they can precisely determine: **(i)** the signature of all VOCs of the disease breathprint
33 on the SiNW FET sensor; **(ii)** correlation between the sensor's sensitivity and
34 specificity of the disease breathprint to its existence in a population of patients; and
35 **(iii)** the necessary feedback that accounts for confounding factors, such patients'
36 diet, metabolic state, genetics, *etc.*
37
38
39
40
41
42
43
44
45

46 For the clinical study, 2 kinds analysis were carried out: ANN analysis and
47 discriminant function analysis (DFA). As mentioned earlier, ANNs are a machine-
48 learning method inspired by biological neural networks (*i.e.* the human nervous
49 system). It is based on a set of functions connecting the input (sensor features in this
50 case) with the output (classification of samples to a specific disease). On the other
51 hand, DFA is a linear supervised pattern recognition method that effectively reduces
52 the multidimensional experimental data, in which the classes to be discriminated are
53 defined, before carrying out the analysis. More details on these approaches and their
54 implementation in the clinical study can be found in the Experimental Methods
55
56
57
58
59
60

section. Using one or both of these approaches, the aim was to distinguish between breathprints of patients belonging to the 4 study groups (**Figure 4**).

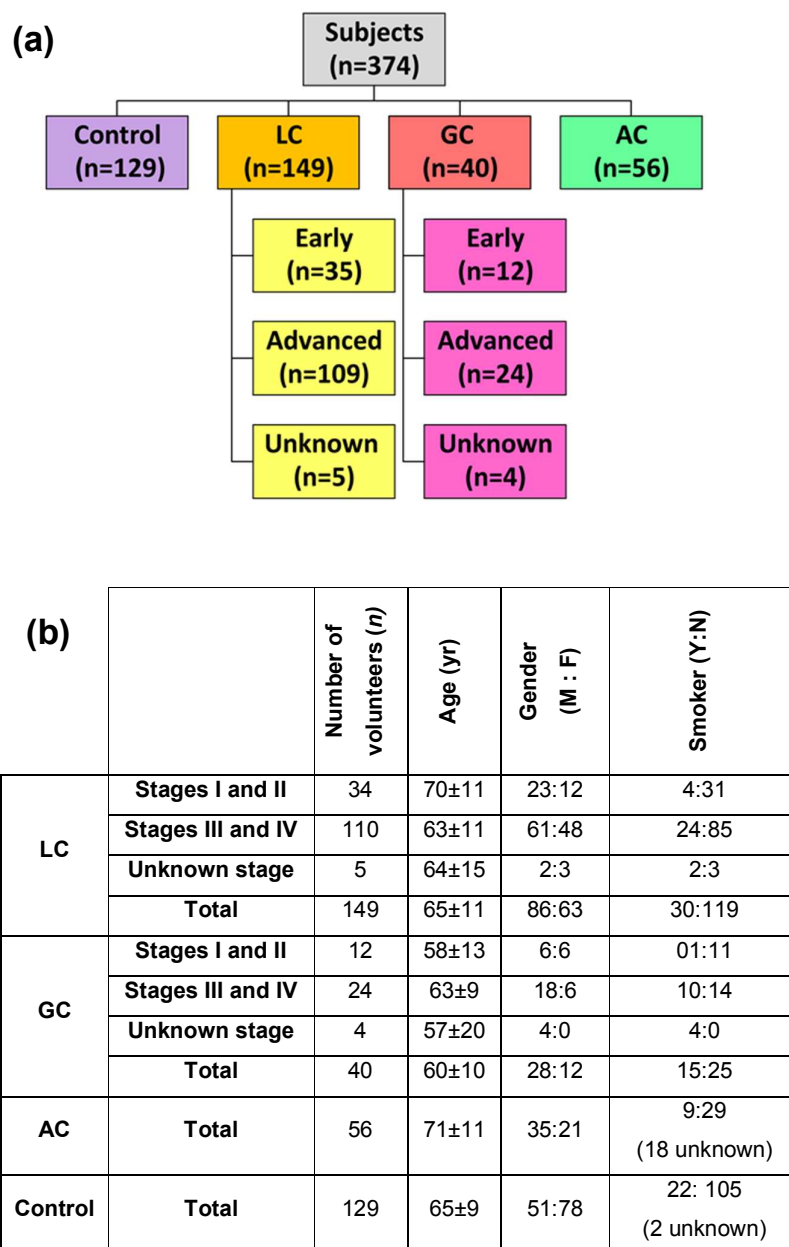


Figure 4. (a) Division of subjects into the groups. The 374 subjects who provided breath samples were separated into the following groups: healthy control volunteers (n=129), LC patients (n=149), GC (n=40) patients and AC patients (n=56). Cancer patients were further separated into 2 groups according to the disease stage: Early and advanced. (b) Full clinical details including age, gender, smoking status and as r classification into one of the groups given in (a).

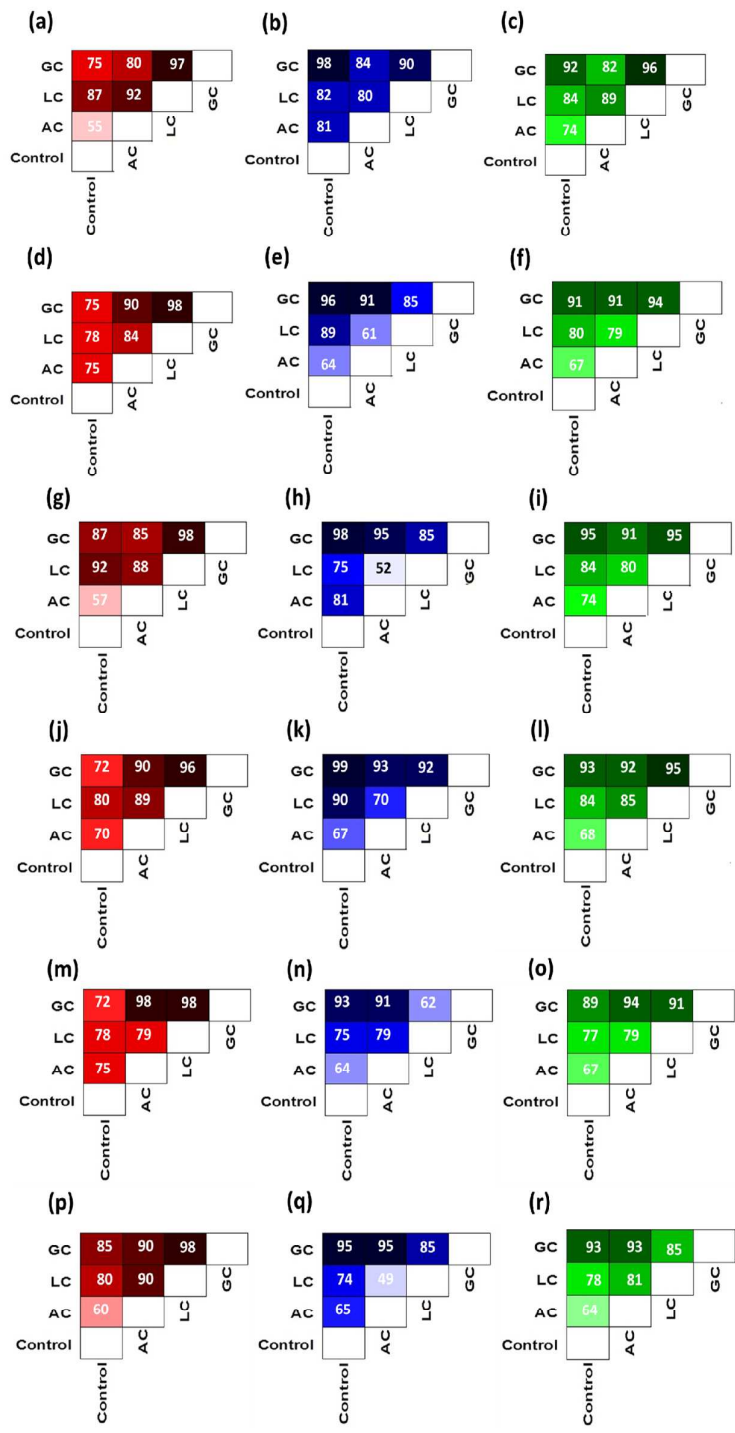


Figure 5. Sensitivity (red; a, d, g, j, m, p), specificity (blue; b, e, h, k, n, q) and accuracy (green; c, f, i, l, o, r) for binary comparisons between the response of S1-S6 to breath samples of volunteers from all groups: LC, GC, AC and healthy control. Classification was obtained by ANN analysis (each row corresponds to a different sensor- top row (a, b, c) corresponds to S1, the second (d, e, f) to S2, etc.). In this classification, all stages of a disease were considered as one group (without staging). Numbers in white are the values, e.g. the value in the red box relating GC and control is the sensitivity of their comparison; the

1
2
3 value in the blue box is the specificity and in the green box is the accuracy. **NOTE:** In
4 comparing any of the groups with the "control" group, the latter was clearly considered the
5 "negative" group, while the others were considered the "positive" groups. In comparing one of
6 the cancer groups (LC or GC) to AC, former was considered the "positive" and AC the
7 "negative" group. Finally, in comparing the 2 types of cancer, LC was taken as the "positive"
8 group, and GC the "negative" group. The values of the comparisons are reviewed in
9 Supporting Information **Table S3**.
10
11
12

13
14
15 **Figure 5** presents the sensitivity, specificity and accuracy values as
16 determined by ANN analysis for binary comparisons between breathprint of
17 volunteers from all groups. Most sensors had an acceptable ability to classify the
18 different diseases, distinguishing them from the control samples. S1, S3 and S5 have
19 the highest ability of to classify correctly breathprints. In trying to separate the LC
20 from the control group, S1 was the most suitable sensor, with sensitivity, specificity
21 and accuracy all >80% (sensitivity 87%, specificity 82% and accuracy 84%). In trying
22 to separate GC patients from the control group, S3 had greater sensitivity than S1,
23 sensitivity 87%, specificity 98%, and accuracy 95%. Regarding AC, when the goal
24 was to rule in a subject (meaning the patient was most likely sick and the test being
25 used as confirmation), the sensor of choice was S1 (specificity 81%). When the goal
26 was to rule out a patient, the sensor of choice was S5 (sensitivity 75%). Regarding
27 the separation of LC patients from AC patients (cancer vs. non-cancer), S1
28 discriminated best overall (sensitivity 92%; specificity 80%; and overall accuracy
29 89%) - making it an excellent sensor for ruling out diagnostic decision. Examining
30 the discrimination between GC and AC, most sensors showed noteworthy results
31 (accuracy >80%). Nevertheless, S5 gave the best results, with all 3 statistical
32 parameters >91%, with an especially high sensitivity of 98%. Comparing GC and LC
33 patients, S1 gave the best results, offering extremely high values of sensitivity,
34 specificity and accuracy (97, 90, and 96%, respectively). Looking at the separation
35 ability of all the sensors in the case of AC vs. control, the performance of the sensors
36 was rather low across the board. This could have been to only one VOC (pentane)
37 characterizing these diseases (asthma and COPD; *cf.* **Table 2**) rather than a pattern
38 of VOC, as in the other diseases. Adsorption of a combination of VOCs on the
39 surface of the Si NW sensor led to a higher signal-to-noise ratio.
40
41
42
43
44
45
46
47
48
49
50
51
52

53 The performance of our devices under real-world conditions has several
54 advantages over the current gold standard test. For example, the National Lung
55 Screening Trial found that CT scans were highly sensitive in detecting lung cancer in
56 smokers compared with chest x-rays, but they were not very specific in ruling out
57
58
59
60

1
2
3 malignancy.⁵² Sensitivity was 94% and specificity 73% for lung cancer detection with
4 CT compared with 74% and 91% with chest x-rays in the first round of screening of
5 high-risk smokers and former smokers included in the trial.⁵² This combination led to
6 substantially more positives in the CT group (27 vs. 9%), nearly all of which prompted
7 follow-up diagnostic procedures.⁵² In comparison, the diagnostic performance of S1
8 provided a benefit in being more cost efficient, practical, and efficacious. In another
9 example, upper endoscopy with a full biopsy is the gold standard for diagnosing and
10 screening gastric cancer and the related precancerous lesions.⁵³ However, this is not
11 a feasible screening approach outside Asia and the cost-effectiveness in other this
12 parts of the world has not been assessed. The cost-effectiveness of our sensors
13 would thus be more affordable and give greater compliance for an at-risk population.
14 On the other hand, an acceptable non-invasive test with high diagnostic
15 performances is lacking, since the best available test – detection of pepsinogens in
16 blood – fails to reach the expected accuracy levels – it could be missing in the
17 majority of cancer cases.⁵³ Whilst in population-based screening settings, the
18 sensitivity of pepsinogen tests is 67-85% and the specificity 76-87% for the detection
19 of atrophy, the sensitivity of gastric cancer detection is only 37-62%.⁵³ In comparison
20 to these values, S3, for example, is the frontrunner for clinical use as population-
21 based diagnostic or screening tool.

22
23
24
25
26
27
28
29
30
31
32 To further validate the analysis, the same binary comparisons were carried by
33 discriminant function analysis (DFA). The data were similar to the ANN results, with
34 S1 being the most adequate sensor for disease classification in most cases, coupled
35 with S3 and S4 for the remaining classifications (LC vs. control and LC vs. AC).
36 Results of the DFA analysis are given in Supporting Information, **Figure S1 and**
37 **Table S4**. It is worthy to point out that looking at the DFA results (Figure S1), we get
38 a different picture than received in using ANN. In the case of DFA, it is S3 that has
39 the best results for discriminating between GC and the other two diseases, resulting
40 in an accuracy of 95%. When comparing GC with the control group, we get an
41 accuracy of 93%, which is very high, but S4 showed better results (accuracy of 94%)
42 due to a higher sensitivity. When studying the differentiation of LC from the control
43 group, we can see that a combination of S3 and S4 should be used, as S3 has a high
44 value of specificity (87%), and S4 has a high sensitivity value (90%). Therefore, S3
45 should be used as a ruling in tool, while S4 would be used for ruling out. Separating
46 the cancerous lung conditions from the non-cancerous lung conditions (AC), S4 is
47 the most suitable sensor as it has extremely high values of sensitivity, specificity and
48 accuracy (89% sensitivity, 75% specificity, and 86% accuracy). The last comparison
49 to be made is the AC group and the control group. In this case, we can see low
50
51
52
53
54
55
56
57
58
59
60

1
2
3 sensitivity values all across the board, similarly to the values received when using
4 ANN. Despite that fact, we still have satisfactory accuracy values, due to the high
5 specificity. The most suitable sensor to be used in this case is either S3 or S4, as
6 they both exhibited the highest specificity and accuracy values (91% and 78%
7 accordingly).
8
9

10
11 Following the very successful classification of the breathprints in the clinical
12 study, we used DFA to classify breath samples collected from cancer patients
13 according to the stage of the disease. For this comparison, DFA was preferred to
14 ANN because the latter does not provide reliable results with small size
15 populations.⁵⁴ The best results were achieved in the DFA model built by using
16 features extracted from S4 for both LC and GC staging (**Table 4**). During the
17 development of the staging models, early stages were considered to be the positive
18 group and the advanced stages negative, which means that the sensitivity indicates
19 detection at the early stage, whereas the specificity is related to advanced stage
20 detection. Classification of the results in the staging analysis by DFA are shown in
21 **Figure 6**. In interpreting this data, DFA classification gave an accuracy of 81% for LC
22 staging and 87% for GC staging. In LC staging, the sensitivity value was low (34.5%),
23 most likely due to the difference in the size of the groups (n=34 for early stage
24 patients and n=110 for the advanced stage). Indeed, big differences in the group size
25 leads to the result being biased towards the larger group, leading to a lack of
26 sensitivity.⁵⁵ Despite low sensitivity, the specificity achieved by S4 was very high
27 (95%), being the highest accuracy value. Regarding the GC staging results, S4
28 showed an equally high ability in identifying both early and advanced stages of the
29 disease (86.5% of the samples were correctly classified; 84.6% of the early stage;
30 and 87.5% of the advanced stage). The AUC values of the classification achieved by
31 S4 were calculated as 0.68 for LC staging and 0.87 for GC staging. ROC curves
32 developed for the separation of each stage from the negative samples can be found
33 in Supporting Information, **Figure S2**. Clear differences were seen between each set
34 of ROC curves (early vs. negative compared to advanced vs. negative) and the
35 different diseases.
36
37
38
39
40
41
42
43
44
45
46
47
48
49
50
51
52
53
54
55
56
57
58
59
60

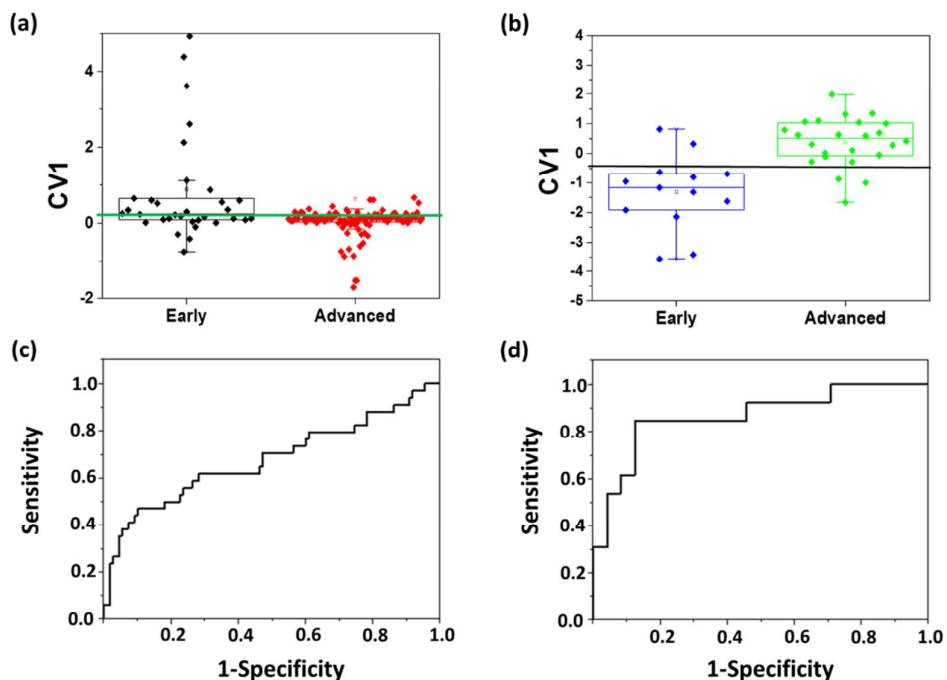


Figure 6. Box plot of the first canonical variable (CV1) values in the staging of (a) LC and (b) GC, as calculated using the S4 DFA model. The box represents 95% confidence interval of CV values; error bars represent the standard deviation. The central lines represent Youden's cut-point. "Early" stages refer to stages 1 and 2 of the disease (localized tumors), and "advanced" are stages 3 and 4 (metastasized tumors). Receiver operating characteristic (ROC) curves (c&d) are also presented. The P-values of these discriminations were 0.0017 for (c) LC and (d) 0.033 for GC (d).

Table 4: Summary of sensitivity, specificity and accuracy values achieved from DFA analysis for the staging of lung cancer (LC) and gastric cancer (GC)

	S1			S2			S3			S4			S5			S6		
	Sensitivity (%)	Specificity (%)	Accuracy (%)	Sensitivity (%)	Specificity (%)	Accuracy (%)	Sensitivity (%)	Specificity (%)	Accuracy (%)	Sensitivity (%)	Specificity (%)	Accuracy (%)	Sensitivity (%)	Specificity (%)	Accuracy (%)	Sensitivity (%)	Specificity (%)	Accuracy (%)
LC-Staging	20.6	94.5	77.1	26.5	88.2	73.6	32.5	94.5	79.9	35.3	94.5	80.6	35.3	90.9	77.8	29.4	88.2	74.3
GC- Staging	53.8	83.3	73	61.5	83.3	75.7	77	80	78.4	84.6	87.5	86.5	53.8	83.3	73	53.9	87.5	85.7

Summary and Conclusions:

Molecularly-modified SiNW FETs linked with pattern recognition methods and/or machine learning have successfully demonstrated the detection and classification of several disease breathprints from lung cancer, gastric cancer, asthma and Chronic Obstructive Pulmonary Disease patients, both under lab and clinical conditions. SiNW FET coated with trichloro(phenethyl)silane (TPS) (S1) and heptanoyl chloride (S3) could detect VOCs linked with the breathprint of the diseases and distinguish one from another. These sensors could separate early stages of cancer from advanced stages, allowing not only the detection of the disease, but estimation of its progress. This information can supply clinicians with valuable and useful information in diagnosis and treatment planning without the necessity of causing patients discomfort or pain, preventing time delay and reducing the financial cost incurred by the clinic/hospital. S1 and the others giving satisfying performances (*e.g.*, S5) could serve as translational tools from fundamental research to point-of-care because the sensors are significantly smaller, easier-to-use, and less expensive than other sensing approaches. They could be used as point-of-care and wearable diagnostic devices. But this pilot study does not allow us to draw far-reaching conclusions. A multi-center clinical trial with a considerably increased sample size, using Si NW FET sensors that enable *in-situ* sampling and analysis, is required to confirm the breathprints. We believe the reported SiNW FET sensor can be modified for selective VOC recognition and concentration prediction in other cancer or disease states.

Experimental Methods

Growth of the SiNWs

P-type silicon nanowires (SiNWs) were grown following the vapor liquid solid (VLS) principle using a cold-wall chemical vapor deposition (CVD) reactor. During the 30 min CVD process under a total pressure of 2 mbar, the flow rates of SiH₂, B₂H₆ (100 ppm in H₂), and Ar were kept constant at 4, 1, and 10 sccm, respectively, *i.e.* in a B to Si ratio of 1:20,000. Growth was catalyzed by commercially available Au colloids (British Biocell Int.) of 30 nm diameter. Growth substrate temperature was ~500°C. The resulting SiNWs had an average diameter of 40±8nm and average length of 8.5±1.5 μm.

Deposition of the SiNWs array

The as-grown SiNWs were first immersed in a KI/I₂/H₂O solution (mass ratio 4:1:40) for 1 min to remove the gold catalyst used in the growing process, and any possible gold contaminants remaining on the surface of the SiNW. The Si NWs were etched using buffered hydrofluoric acid for 10 sec. Following this, the SiNWs were dispersed in ethanol using ultra-sonication for 5 sec, and were later deposited on a highly-doped (0.001 Ω·cm resistivity) P-type Silicon (100) substrate with 300 nm thermal oxide and a Ti/Au (10/200 nm) bottom gate electrode. Deposition was based on a spray-coating procedure,⁵⁶ which started with the deposition of the substrate on a hotplate set at 75°C. A SiNW suspension was applied with a spray gun (PRONA R2F) at a carrier gas pressure of 40 psi, and a tilt angle of (5°±2°) to the substrate. The spray-coating process resulted in well-aligned nanowire arrays (density ~ 1 NW/100 μm²).

Fabrication of SiNW FETs

The substrate coated with SiNWs was cleaned by successive immersions in acetone, methanol, and isopropanol, followed by 5 sec rinsing in buffered HF. The top source and drain electrodes (20 pairs of 20 nm Ti/ 160 nm Au interdigitated electrodes, length 1300 μm, width 2 μm, spacing 2 μm) were deposited by a photolithography (Karl Suss MA6 Mask aligner) and lift-off process on top of the SiNWs. Surface characterization of the fabricated used dark-field light microscopy to determine the density of SiNWs on the device, which were then observed in a scanning electron microscope (SEM) to assure proper contact between the SiNWs and the electrodes.

Surface modification of the SiNW FETs

Surface modification of the SiNW FETs was carried as described before.⁴³ Briefly, following surface activation achieved by 30 sec of plasma treatment, the SiNW FET surfaces were modified with various molecules (listed in Table 1). SiNW FETs were modified using a single-step silane modification (SSM), a 2-step silane-chloride modification (TSCM), or a 2-step silane-monomer modification (TSMM). Devices modified using the SSM approach were: (i) immersed in a silane/chloroform (silane/ethanol in case of APTES) solution (2 mM; 10 mL) for 45 min in room temperature, and then (ii) successively rinsed with chloroform, acetone, ethanol, isopropanol (ethanol, acetone, ethanol and isopropanol in case of APTES) and drying by N₂ flow. The silane molecules prepared by this SSM approach and used in this study were trichloro(3,3,3-trifluoropropyl)silane (CF₃CH₂CH₂SiCl₃; TTPS), trichloro(phenethyl)silane (C₆H₅CH₂SiCl₃; TPS), 3-aminopropyl-triethoxysilane (C₉H₂₃NO₃Si; APTES) and 3-bromopropyl trichlorosilane (C₃H₆BrCl₃Si; BPTS). SiNW FETs modified using the TSCM approach were: (i) immersed in 3-aminopropyl-triethoxysilane (APTES)/dehydrated ethanol (10 mM, 20 mL) for 1 h, (ii) rinsed with ethanol, acetone, isopropanol and dried by N₂ flow, (iii) immersed in a solution of acylchloride in chloroform (10 mM) with 10 μL of triethylamine for 17 h, and finally, (iv) successively rinsed with chloroform, acetone, ethanol, and isopropanol before being dried by N₂ flow. The molecular modification prepared by the TSCM approach was heptanoyl chloride (C₇H₁₃ClO). SiNW FETs modified using TSMM were: (i) immersed in trichloro(3,3,3-trifluoropropyl)silane (CF₃CH₂CH₂SiCl₃; TTPS)/chloroform (2 mM, 10 mL) for 1 h, (ii) successively rinsed with chloroform, acetone, ethanol and isopropanol, before being dried by N₂ flow, (iii) drop-casted with a monomer solution in tetrahydrofuran (THF) (1 mM, 2 μL) and kept in a vacuum oven overnight (55°C), and (iv) rinsed with THF, acetone, ethanol and isopropanol before drying in a N₂ flow. The molecular modification prepared by the TSMM approach was anthracene (C₁₄H₁₀).

Breath sample collection

Exhaled alveolar breath samples from 374 volunteers were collected. The volunteers were divided into 4 groups: 149 volunteers with lung cancer; 40 with gastric cancer; 56 volunteers with non-cancerous lung diseases (asthma, COPD or both); and 129 volunteers who were negative for all these diseases. These samples were collected in 4 locations: **(i)** Riga East University Hospital, Riga, Latvia; **(ii)** Cancer Research Center, University of Liverpool, Liverpool, UK; **(iii)** Thoracic Cancer Research and Detection Center, Sheba Medical Center, Tel-Hashomer, Israel; and **(iv)** Baptist

1
2
3 Cancer Institute, Jacksonville, Florida, USA. A summary of the clinical data is
4 presented (**Figure 4b**).
5

6 In each location, the samples were collected in the same hospital room.
7 Patients were asked to fast, and withhold smoking and alcohol consumption for at
8 least 2 h before sampling. The sorbent tubes were stored at 4°C until transported to
9 Laboratory of Nanomaterial Based Devices (Technion – Israel Institute of
10 Technology, Haifa, Israel) for analysis. The duration between sample collection and
11 analysis was <3 months (NOTE: breath VOCs can be preserved in these sorbent tubes
12 up to 6 months without change in their composition). The breath samples were
13 collected following a previously described protocol^{14,57}. To reduce the effect of
14 ambient contamination, a lung washout procedure was used. According to the
15 protocol, the patient took regular, unexerted breaths for 3 min through a mouthpiece
16 with a filter cartridge on the inspiratory port (Eco Medics, Duerten, Switzerland),
17 thereby greatly reducing the concentration of ambient VOCs in the inspired air.
18 **NOTE:** The subjects were asked to breathe normally throughout the entire procedure
19 to avoid hyperventilation. Following lung washout, the subjects were asked to inhale
20 normally once more through the filter and exhale normally through the mouthpiece
21 into a separate exhalation port against 10-15 cm H₂O pressure (ensuring the closure
22 of the vellum to exclude contamination through nasal entrainment). During
23 exhalation, the respiratory dead space air is first exhaled, the alveolar air coming
24 thereafter. The dead-space air was automatically filled into a designated bag at the
25 beginning of the exhalation and was later removed. The alveolar breath from the tidal
26 end was filled into breath collection bags (China: TedlarR bags, Keika Ventures, LLC;
27 Latvia: Mylar bags, Quintron, Milwaukee, WI, USA). The breath collection method
28 applied is a single-step process; the volunteer does not have to take care of
29 exchanging the dead space bag with the collection bag. Following the collection
30 procedures, the breath samples were transferred to ORBOTM 402 Tenax sorption
31 tubes (specially treated; 35/60 mesh; 100/50 mg; from Sigma-Aldrich, USA) by
32 pumping each sample through a sorbent tube. We have confirmed that the VOCs in
33 the breath of lung cancer patients and other lung conditions can be trapped and
34 stored in the ORBOTM 402 Tenax® TA sorption tubes.
35
36
37
38
39
40
41
42
43
44
45
46
47
48
49
50

51 ***Breath analysis with the SiNW FET sensors***

52 A manual thermal desorption (TD) system was used to transfer the VOCs trapped in
53 the disposable sorbent tubes. Each tube was heated at 190°C for 8 min under a
54 constant N₂ (99.999% purity) flow at 60 ml/min to release the trapped breath VOCs
55 into the bag. A pulse of the content of the bags was delivered into a stainless steel
56
57
58
59
60

1
2
3 test chamber containing the SiNW FET sensors described in Table 1. A Keithley
4 2636A system sourcemeter and a Keithley 3706 system switch/MultiMeter were used
5 to measure the I_{ds} - V_{gs} (back sweep from +40 to -40V; in steps of 200 mV and
6 constant V_{ds} of 2V) as a function of time. For each sample, the baseline responses of
7 the sensors were recorded, first for 10 min in vacuum (30 mTorr), followed by 10 min
8 exposure of the breath sample, and 10 min during the recovery of the sensors. To
9 detect malfunctions and/or slight drifts of their baseline conditions, the sensors were
10 calibrated daily by exposure to known concentrations of three calibration compounds,
11 including 23.8 ppm isopropyl alcohol, 6.3 ppm trimethylbenzene, and 1.2 ppm 2-
12 ethylhexanol before recording their resistance changes. Sensing features were read
13 out and extracted from the time-dependent response of each sensor that related to
14 voltage threshold (V_{th}), hole mobility (μ_h), and source-drain current (I_{sd}) at various
15 back gate voltage (V_{gs}) features. Breath patterns were obtained from the collective
16 response of the sensors by applying discriminant factor analysis (DFA) and artificial
17 neural networks (ANNs).
18
19
20
21
22
23
24
25
26
27
28

29 **Artificial Neural Networks (ANNs)**

30 ANNs is a machine-learning method inspired by neural networks in the human
31 nervous system. It is based on a set of functions connecting the input (sensor
32 features in this case) with the output (classification of samples to a specific disease).
33 This relationship is achieved by optimizing certain parameters - connection weights,
34 and amount of neurons (calculation centers) - to achieve the best classification from
35 the inputs available. To reach the final mathematical binary classifying models to
36 distinguish between the 4 groups of participants (LC, GC, Asthma/COPD, and
37 negative to all), a 2-phase calculation process was used. The same steps were
38 carried out for every available database (one per sensor (6) and possible binary
39 classifier (6); a total of 36 models). Initially, a feature selection (FS) procedure was
40 used to determine the sensing features with the greatest discriminative power to
41 identify correctly the samples within a particular dataset. FS calculation was based
42 on the Relief-F algorithm, which is a filter FS method. It operates by locating the
43 nearest neighbors of a sample in its same class and other classes, giving priority to
44 those features that distinguish better the nearest neighbors from different classes.⁵⁸
45 FS leads to the location of the best suited variables (sensing features in this case) to
46 fulfil a second modeling phase, which leads to a reduced computational load and
47 improved performance of further models.⁵⁹ The second part of the calculation is the
48 modeling phase; using the features given by the FS test as independent variables, a
49
50
51
52
53
54
55
56
57
58
59
60

1
2
3 set of 36 multilayer perceptrons (MLPs), which are the most employed type of neural
4 network, were designed and optimized. Based on non-linear interpolation for the
5 calculations, MLPs are supervised algorithms, or in other words, tools that require
6 target data (labelled data) to be trained properly.⁶⁰ In this case, the samples for every
7 binary classifier were either tagged with a zero or a one depending on the group they
8 belonged to. These labels become the dependent variable of each MLP classifier.
9 MLPs, as their name suggests, are layered algorithms, possessing 3 kinds of layers
10 (input, hidden and output). The input layer is formed by nodes that are only in charge
11 of introducing the independent variables of the model (the sensing features selected
12 during the FS phase). On the other hand, the hidden and output layers are formed by
13 neurons, which are in charge of the calculations of the system. The number of
14 neurons in the output layer are equivalent to the amount of dependent variables in
15 the system (one in this case, as all the models are binary classifiers), whereas the
16 hidden neuron number (HNN) (*vide infra*) and hidden layer amount must be correctly
17 optimized (due to the size of the databases, the amount of hidden layers was set to
18 one in all cases to avoid over-fitting).⁴⁸ Once the number of units (nodes and
19 neurons) in each layer or network topology has been defined, the training process of
20 the MLP can begin. The goal of this process is to optimize the weights that are
21 contained within the model, there being as many weights as connections between
22 units in neighboring layers (node-hidden neurons and hidden neurons-output
23 neurons). The correct optimization of the weights is vital for a MLP to operate
24 correctly, and this process is carried out during a series of training cycles or epochs.
25 These cycles modify the values of the weights, with the goal set to lower the error of
26 the estimation for a training dataset (in our case, to increase the correct classification
27 ratio). This error can potentially reach zero if no precautions are followed, leading to
28 an over-fit model. For this reason, the total database is initially divided into training
29 and verification datasets, where the first is used to modify the weights, and the latter
30 to verify that the MLP can perform well with samples that are not involved in this
31 process. When the error for the verification dataset rises during 6 straight epochs, the
32 training process is stopped, and the model is optimized as well as being not over-fit
33 towards the training samples.⁶¹ Besides the weights, there are other parameters that
34 have to be correctly selected or optimized to reach a fully operational MLP. They are
35 the HNN, the training and transfer functions, and a set of network parameters
36 (Marquardt adjustment parameter (Lc), decrease factor for Lc (Lcd), and increase
37 factor for Lc (Lci)), as follows. First, optimizing the HNN is crucial, as an excessive
38 amount will most likely create over-fit models, and a low one will not allow the MLP to
39 reach its maximum calculating potential; it has been optimized heuristically during
40
41
42
43
44
45
46
47
48
49
50
51
52
53
54
55
56
57
58
59
60

1
2
3 this research.⁶² Second, the training function is in charge of the calculations that
4 modify the weights. The one chosen here was the Levenberg-Marquardt (trainLM)
5 function as it is the quickest algorithm for moderate-sized MLPs and has a memory
6 reduction feature where the training dataset is large.⁶² Third, the transfer function is
7 in charge of introducing non-linearity in the calculations, as well as limiting the range
8 of the values of the responses given by each neuron. The selected option was the
9 sigmoid function, which limits the values between zero and one.⁵⁴ Finally, the Lc
10 parameter is analogous to the learning coefficient in classic back-propagation
11 algorithm;⁶³ its value decreases and increases with Lcd and Lci, respectively, until the
12 modifications of Lc create a worse statistical performance.
13
14
15
16
17
18
19

20 ***Discriminant Factor Analysis (DFA)***

21 DFA is a linear, supervised pattern recognition method that effectively reduces the
22 multidimensional experimental data, in which the classes to be discriminated are
23 defined before the analysis is performed. First, DFA was used for the selection of the
24 sensors with the most relevant organic functionality out of a repertoire of 20, which
25 was done by filtering out non-contributing sensors. DFA determines the linear
26 combinations of the input variables (features being extracted from each sensor), so
27 the variance in each class is minimized and that between classes maximized. The
28 DFA output variables (*i.e.* canonical variables - CV) are achieved in mutually
29 orthogonal dimensions; the first CV is the most powerful discriminating dimension.
30 Leave-one-out cross-validation was conducted in calculating the classification
31 success in terms of sensitivity, specificity and accuracy calculated as follows:
32
33
34
35
36
37
38
39

$$40 \text{ Sensitivity} = \frac{TP}{TP+FN} \quad (1)$$

$$41 \text{ Specificity} = \frac{TN}{TN+FP} \quad (2)$$

$$42 \text{ Accuracy} = \frac{TP+TN}{Total} \quad (3)$$

43
44
45
46
47
48
49 Where TP stands for true positive, namely all positive samples correctly classified as
50 positive; TN (true negative) - negative samples correctly classified as such; FP (false
51 positive) - the negative sample incorrectly classified as positive; FN (false negative) -
52 positive samples incorrectly classified as negative; and "total" is the total number of
53 samples. Given k, the model was computed using k-1 training vectors. All
54 possibilities of leave-one-sample-out were considered, and the classification
55
56
57
58
59
60

1
2
3 accuracy was estimated as the averaged performance over the k tests. Pattern
4 recognition and data classification used MATLAB® (The MathWorks).
5
6
7
8
9

10 **ASSOCIATED CONTENTS:**

11 **Supporting Information**

12
13 Analytical values of the VOCs in the exhaled breath of patients and limit of detection
14 of the examined sensors, statistical performance of every MLP model, summary of
15 sensitivity / specificity / accuracy values achieved from DFA analysis of the samples,
16 ROC curves for staging of LC and GC, are all available free of charge on the Internet:
17 <http://pubs.acs.org>.
18
19
20
21
22
23

24 **Corresponding Author**

25
26 * H. Haick. Email: hossam@technion.ac.il
27
28
29
30

31 **Acknowledgments**

32 This research received funding from the FP7-Health Program under the LCAOS
33 (grant agreement no. 258868) and from the Horizon 2020 ICT Program under the
34 SNIFFPHONE (grant agreement no. 644031). Clinical sample collection in Latvia
35 was funded in part from the grant No. 305/2012 from the Latvian Council of Science.
36 Fabrication was performed at the Micro-Nano Fabrication Unit (MNFU) of the
37 Technion – Israel Institute of Technology. The authors acknowledge Mr. Alaa Gharra
38 for assistance with statistical analysis and Dr. Viki Klopper for help in part of the
39 schematics.
40
41
42
43
44
45
46
47

48 **Competing financial interests**

49 The authors declare no competing interests.
50
51
52
53

54 **References:**

- 55 1. Siegel, R. L.; Miller, K. D.; Jemal, A. Cancer Statistics, 2015. *CA: A Cancer J. Clin.* **2015**,
56 65, 5-29.
57
58
59
60

2. Gibson, P. G.; Simpson, J. L. The Overlap Syndrome of Asthma and COPD: What Are Its Features and How Important Is It? *Thorax* **2009**, *64*, 728-735.
3. Broza, Y. Y.; Mochalski, P.; Ruzsanyi, V.; Amann, A.; Haick, H. Hybrid Volatolomics and Disease Detection. *Angew. Chem. Int. Ed.* **2015**, *54*, 11036-11048.
4. Haick, H.; Broza, Y. Y.; Mochalski, P.; Ruzsanyi, V.; Amann, A. Assessment, Origin, and Implementation of Breath Volatile Cancer Markers. *Chem. Soc. Rev.* **2014**, *43*, 1423-1449.
5. Nakhleh, M.; Broza, Y. Y.; Haick, H. Monolayer-Capped Gold Nanoparticles for Disease Detection from Breath. *Nanomedicine (London, UK)* **2014**, *9*, 1991-2002.
6. Amal, H.; Leja, M.; Funka, K.; Skapars, R.; Sivins, A.; Ancans, G.; Liepniece-Karele, I.; Kikuste, I.; Lasina, I.; Haick, H. Detection of Precancerous Gastric Lesions and Gastric Cancer Through Exhaled Breath. *Gut* **2016**, *65*, 400-407
7. Amal, H.; Leja, M.; Funka, K.; Lasina, I.; Skapars, R.; Sivins, A.; Ancans, G.; Kikuste, I.; Vanags, A.; Tolmanis, I.; Kirsners, A.; Kupcinskas, L.; Haick, H. Breath Testing as Potential Colorectal Cancer Screening Tool. *Int. J. Cancer* **2016**, *138*, 229-236.
8. Amal, H.; Shi, D.-Y.; Ionescu, R.; Zhang, W.; Hua, Q.-L.; Pan, Y.-Y.; Tao, L.; Liu, H.; Haick, H. Assessment of Ovarian Cancer Conditions from Exhaled Breath. *Int. J. Cancer* **2015**, *136*, E614-E622.
9. Ionescu, R.; Broza, Y.; Shaltieli, H.; Sadeh, D.; Zilberman, Y.; Feng, X.; Glass-Marmor, L.; Lejbkowicz, I.; Müllen, K.; Miller, A.; Haick, H. Detection of Multiple Sclerosis from Exhaled Breath Using Bilayers of Polycyclic Aromatic Hydrocarbons and Single-Wall Carbon Nanotubes. *ACS Chem. Neurosci.* **2011**, *2*, 687-693.
10. Tisch, U.; Schlesinger, I.; Ionescu, R.; Nassar, M.; Axelrod, N.; Robertman, D.; Tessler, Y.; Marmur, A.; Aharon-Peretz, J.; Haick, H. Detection of Alzheimer's and Parkinson's Diseases from Exhaled Breath Using Nanomaterial-Based Sensors. *Nanomedicine (London, UK)* **2013**, *8*, 43-56.
11. Konvalina, G.; Haick, H. The effect of Humidity on Nanoparticle-Based Chemiresistors: A Comparison Between Synthetic and Real-World Samples. *ACS Appl. Mater. Interfaces* **2012**, *4*, 317-325.
12. Nakhleh, M. K.; Amal, H.; Awad, H.; Gharra, A.; Abu-Saleh, N.; Jeries, R.; Haick, H.; Abassi, Z. Sensor Arrays Based on Nanoparticles for Early Detection of Kidney Injury by Breath Samples. *Nanomedicine (New York, NY, US)* **2014**, *19*, 00320-00327.
13. Nakhleh, M. K.; Jeries, R.; Gharra, A.; Binder, A.; Broza, Y. Y.; Pascoe, M.; Dheda, K.; Haick, H. Detecting Active Pulmonary Tuberculosis with a Breath Test using Nanomaterial-Based Sensors. *Eur. Respir. J.* **2014**, *43*, 1522-1525.
14. Xu, Z. q.; Broza, Y. Y.; Ionsecu, R.; Tisch, U.; Ding, L.; Liu, H.; Song, Q.; Pan, Y. Y.; Xiong, F. X.; Gu, K. S.; Sun, G. P.; Chen, Z. D.; Leja, M.; Haick, H. A Nanomaterial-Based Breath Test for Distinguishing Gastric Cancer from Benign Gastric Conditions. *Br. J. Cancer* **2013**, *108*, 941-950.

15. Hakim, M.; Billan, S.; Tisch, U.; Peng, G.; Dvorkind, I.; Marom, O.; Abdah-Bortnyak, R.; Kuten, A.; Haick, H. Diagnosis of Head&Neck Cancer from Exhaled Breath. *Br. J. Cancer* **2011**, *104*, 1649-1655.
16. Amann, A.; Mochalski, P.; Ruzsanyi, V.; Broza, Y. Y.; Haick, H. Assessment of the Exhalation Kinetics of Volatile Cancer Biomarkers Based on their Physicochemical Properties. *J. Breath. Res.* **2014**, *8*, 016003.
17. Hakim, M.; Broza, Y. Y.; Barash, O.; Peled, N.; Phillips, M.; Amann, A.; Haick, H. Volatile Organic Compounds of Lung Cancer and Possible Biochemical Pathways. *Chem. Rev.* **2012**, *112*, 5949-5966.
18. Konvalina, G.; Haick, H. Sensors for Breath Testing: From Nanomaterials to Comprehensive Disease Detection. *Acc. Chem. Res.* **2013**, *47*, 66-76.
19. Phillips, M.; Cataneo, R. N.; Cummin, A. R. C.; Gagliardi, A. J.; Gleeson, K.; Greenberg, J.; Maxfield, R. A.; Rom, W. N. Detection of Lung Cancer with Volatile Markers in the Breath. *Chest* **2003**, *123*, 2115-2123.
20. Simenhoff, M. L.; Burke, J. F.; Saukkonen, J. J.; Ordinario, A. T.; Doty, R.; Dunn, S. Biochemical Profile of Uremic Breath. *New. Eng. J. Med.* **1977**, *297*, 132-135.
21. Phillips, M. Detection of Carbon Disulfide in Breath and Air: A Possible New Risk Factor for Coronary Artery Disease. *Int. Archiv. Occup. Env. Health* **1992**, *64*, 119-123.
22. Wang, C.; Sahay, P. Breath Analysis Using Laser Spectroscopic Techniques: Breath Biomarkers, Spectral Fingerprints, and Detection Limits. *Sensors* **2009**, *9*, 8230-8262.
23. Risby, T. H.; Solga, S. F. Current Status of Clinical Breath Analysis. *Appl. Phys. B* **2006**, *85*, 421-426.
24. Miekisch, W.; Schubert, J. K. From Highly Sophisticated Analytical Techniques to Life-Saving Diagnostics: Technical Developments in Breath Analysis. *TrAC Trends Anal. Chem.* **2006**, *25*, 665-673.
25. Martin, A. N.; Farquar, G. R.; Jones, A. D.; Frank, M. Human Breath Analysis: Methods for Sample Collection and Reduction of Localized Background Effects. *Anal. Bioanal. Chem.* **2010**, *396*, 739-750.
26. Bajtarevic, A.; Ager, C.; Pienz, M.; Klieber, M.; Schwarz, K.; Ligor, M.; Ligor, T.; Filipiak, W.; Denz, H.; Fiegl, M. Noninvasive Detection of Lung Cancer by Analysis of Exhaled Breath. *BMC Cancer* **2009**, *9*, 348.
27. Machado, R. F.; Laskowski, D.; Deffenderfer, O.; Burch, T.; Zheng, S.; Mazzone, P. J.; Mekhail, T.; Jennings, C.; Stoller, J. K.; Pyle, J. Detection of Lung Cancer by Sensor Array Analyses of Exhaled Breath. *Am. J. Resp. Crit. Care Med.* **2005**, *171*, 1286-1291.
28. Fleischer, M.; Simon, E.; Rumpel, E.; Ulmer, H.; Harbeck, M.; Wandel, M.; Fietzek, C.; Weimar, U.; Meixner, H. Detection of Volatile Compounds Correlated to Human Diseases Through Breath Analysis with Chemical Sensors. *Sens. Actuat. B* **2002**, *83*, 245-249.

- 1
 - 2
 - 3
 - 4
 - 5
 - 6
 - 7
 - 8
 - 9
 - 10
 - 11
 - 12
 - 13
 - 14
 - 15
 - 16
 - 17
 - 18
 - 19
 - 20
 - 21
 - 22
 - 23
 - 24
 - 25
 - 26
 - 27
 - 28
 - 29
 - 30
 - 31
 - 32
 - 33
 - 34
 - 35
 - 36
 - 37
 - 38
 - 39
 - 40
 - 41
 - 42
 - 43
 - 44
 - 45
 - 46
 - 47
 - 48
 - 49
 - 50
 - 51
 - 52
 - 53
 - 54
 - 55
 - 56
 - 57
 - 58
 - 59
 - 60
29. Peled, N.; Hakim, M.; Tisch, U.; Bunn, P. A. J. R.; Miller, Y. E.; Kennedy, T. C.; Mattei, J.; Mitchell, J. D.; Weyant, M. J.; Hirsch, F. R.; Haick, H. Non-Invasive Breath Analysis of Pulmonary Nodules. *J. Thorac. Oncol.* **2012**, *7*, 1528-1533.
30. Vishinkin, R.; Haick, H. Nanoscale Sensor Technologies for Disease Detection via Volatolomics. *Small* **2015**, *11*, 6142-6164.
31. Broza, Y. Y.; Haick, H. Nanomaterial-Based Sensors for Detection of Disease by Volatile Organic Compounds. *Nanomedicine (London, UK)* **2013**, *8*, 785-806.
32. Park, H.; Dan, Y.; Seo, K.; Yu, Y. J.; Duane, P. K.; Wober, M.; Crozier, K. B. Filter-Free Image Sensor Pixels Comprising Silicon Nanowires with Selective Color Absorption. *Nano Lett.* **2014**, *14*, 1804-1809.
33. Wang, B.; Cancilla, J. C.; Torrecilla, J. S.; Haick, H. Artificial Sensing Intelligence with Silicon Nanowires for Ultraselective Detection in the Gas Phase. *Nano Lett.* **2014**, *14*, 933-938.
34. Paska, Y.; Haick, H. Interactive Effect of Hysteresis and Surface Chemistry on Gated Silicon Nanowire Gas Sensors. *ACS Appl. Mater. Interfaces* **2012**, *4*, 2604-2617.
35. Paska, Y.; Stelzner, T.; Tisch, U.; Assad, O.; Christiansen, S.; Haick, H. Molecular Gating of Silicon Nanowire Field Effect Transistors with Nonpolar Analytes. *ACS Nano* **2012**, *6*, 335-345.
36. Paska, Y.; Stelzner, T.; Christiansen, S.; Haick, H. Enhanced Sensing of Nonpolar Volatile Organic Compounds by Silicon Nanowire Field Effect Transistors. *ACS Nano* **2011**, *5*, 5620-5626.
37. Paska, Y.; Haick, H. Controlling Properties of Field Effect Transistors by Intermolecular Cross-Linking of Molecular Dipoles. *Appl. Phys. Lett.* **2009**, *95*, 233103/1-3.
38. Lou, L.; Zhang, S.; Park, W.-T.; Tsai, J. M.; Kwong, D.-L.; Lee, C. Optimization of NEMS Pressure Sensors with a Multilayered Diaphragm Using Silicon Nanowires as Piezoresistive Sensing Elements. *J. Micromechan. Microeng.* **2012**, *22*, 055012.
39. Demami, F.; Ni, L.; Rogel, R.; Salaun, A.-C.; Pichon, L. Silicon Nanowires based Resistors as Gas Sensors. *Sens. Actuat. B* **2012**, *170*, 158-162.
40. Yan, Q.; Wang, Z.; Zhang, J.; Peng, H.; Chen, X.; Hou, H.; Liu, C. Nickel Hydroxide Modified Silicon Nanowires Electrode for Hydrogen Peroxide Sensor Applications. *Electrochim. Acta* **2012**, *61*, 148-153.
41. Halpern, J. M.; Wang, B.; Haick, H. Controlling the Sensing Properties of Silicon Nanowires via the Bonds Nearest to the Silicon Nanowire Surface. *ACS Appl. Mater. Interfaces* **2015**, *7*, 11315-11321.
42. Ahmed, L. B.; Naama, S.; Keffous, A.; Houssein-Bey, A.; Hadjersi, T. H 2 sensing properties of modified silicon nanowires. *Progress in Natural Science: Materials International* **2015**.
43. Kim, Y.; Kim, H. J.; Kim, J. H.; Choi, D. G.; Choi, J. H.; Jung, J. Y.; Jeon, S.; Lee, E. S.; Jeong, J.-H.; Lee, J. Rapid Low-Temperature 3D Integration of Silicon Nanowires on Flexible Substrates. *Small* **2015**, *11*, 3995-4001.

- 1
2
3
4
5
6
7
8
9
10
11
12
13
14
15
16
17
18
19
20
21
22
23
24
25
26
27
28
29
30
31
32
33
34
35
36
37
38
39
40
41
42
43
44
45
46
47
48
49
50
51
52
53
54
55
56
57
58
59
60
44. Wang, H.; Fan, P. H.; Tong, B.; Dong, Y. P.; Ou, X. M.; Li, F.; Zhang, X. H. Hydrogen-Terminated Si Nanowires as Label-Free Colorimetric Sensors in the Ultrasensitive and Highly Selective Detection of Fluoride Anions in Pure Water Phase. *Adv. Funct. Mater.* **2015**, *25*, 1506–1510.
 45. Wang, B.; Haick, H. Effect of Functional Groups on the Sensing Properties of Silicon Nanowires Toward Volatile Compounds. *ACS Appl. Mater. Interfaces* **2013**, *5*, 2289-2299.
 46. Wang, B.; Haick, H. Effect of Chain Length on the Sensing of Volatile Organic Compounds by Means of Silicon Nanowires. *ACS Appl. Mater. Interfaces* **2013**, *5*, 5748-5756.
 47. Ermanok, R.; Assad, O.; Zigelboim, K.; Wang, B.; Haick, H. Discriminative Power of Chemically Sensitive Silicon Nanowire Field Effect Transistors to Volatile Organic Compounds. *ACS Appl. Mater. Interfaces* **2013**, *5*, 11172-11183.
 48. Bashouti, M. Y.; Stelzner, T.; Berger, A.; Christiansen, S.; Haick, H. Covalent Attachment of Alkyl Functionality to 50 nm Silicon Nanowires Through Chlorination / Alkylation Process. *J. Phys. Chem. C* **2009**, *113*, 14823-14828.
 49. Bashouti, M. Y.; Stelzner, T.; Berger, A.; Christiansen, S.; Haick, H. Chemical Passivation of Silicon Nanowires with C1–C6 Alkyl Chains Through Covalent Si–C Bonds. *J. Phys. Chem. C* **2008**, *112*, 19168-19172.
 50. Haick, H.; Ambrico, M.; Ligonzo, T.; Cahen, D. Discontinuous Molecular Films can Control Metal/Semiconductor Junctions. *Adv. Mater.* **2004**, *16*, 2145-2151.
 51. Wang, B.; Huynh, T.-P.; Wu, W.; Hayek, N.; Do, T. T.; Cancilla, J. C.; Torrecilla, J. S.; Nahid, M. M.; Colwell, J. M.; Gazit, O. M.; Puniredd, S. R.; McNeill, C. R.; Sonar, P.; Haick, H. Highly Sensitive Ambipolar Field Effect Transistor-Based Diketopyrrolopyrrole Copolymer for Selective Detection and Discrimination of Xylene Isomers. *Adv. Mater.* **2016**, *28*, 4012-4018.
 52. Team, T. N. L. S. T. R. Results of Initial Low-Dose Computed Tomographic Screening for Lung Cancer. *N. Engl. J. Med.* **2013**, *368*, 1980-1991.
 53. Pasechnikov, V.; Chukov, S.; Fedorov, E.; Kikuste, I.; Leja, M. Gastric Cancer: Prevention, Screening and Early Diagnosis. *World J. Gastroenterol.* **2014**, *20*, 13842-13862.
 54. Knoerzer, K.; Juliano, P.; Roupas, P.; Versteeg, C.: *Innovative Food Processing Technologies: Advances in Multiphysics Simulation*; Wiley-Blackwell: Oxford (UK), 2011.
 55. Dunteman, G. H.: *Introduction to multivariate analysis*; Sage Publications: Thousand Oaks, CA, 1984.
 56. Assad, O.; Leshansky, A. M.; Wang, B.; Stelzner, T.; Christiansen, S.; Haick, H. Spray-Coating Route for Highly Aligned and Large-Scale Arrays of Nanowires. *ACS Nano* **2012**, *6*, 4702-4012.

- 1
2
3 57. Amal, H.; Leja, M.; Broza, Y. Y.; Tisch, U.; Funka, K.; Liepniece-Karele, I.; Skapars, R.;
4 Xu, Z. Q.; Liu, H.; Haick, H. Geographical Variation in the Exhaled Volatile Organic
5 Compounds. *J. Breath Res* **2013**, *7*, 047102.
6
7 58. Wu, B.; Chen, C.; Kechadi, T. M.; Sun, L. A Comparative Evaluation of Filter-Based
8 Feature Selection Methods for Hyper-Spectral Band Selection. *Int. J. Rem. Sens.* **2013**,
9 *34*, 7974-7990.
10
11 59. Chandrashekar, G.; Sahin, F. A Survey on Feature Selection Methods. *Comput. Elect.*
12 *Eng.* **2014**, *40*, 16-28.
13
14 60. Basheer, I. A.; Hajmeer, M. Artificial Neural Networks: Fundamentals, Computing,
15 Design, and Application. *J. Microbiol. Meth.* **2000**, *43*, 3-31.
16
17 61. Torrecilla, J. S.; Tortuero, C.; Cancilla, J. C.; Díaz-Rodríguez, P. Estimation with Neural
18 Networks of the Water Content in Imidazolium-Based Ionic Liquids Using Their
19 Experimental Density and Viscosity Values. *Talanta* **2013**, *113*, 93-98.
20
21 62. Cancilla, J. C.; Díaz-Rodríguez, P.; Matute, G.; Torrecilla, J. S. The Accurate Estimation
22 of Physicochemical Properties of Ternary Mixtures Containing Ionic Liquids *via* Artificial
23 Neural Networks. *Phys. Chem. Chem. Phys.* **2015**, *17*, 4533-4537.
24
25 63. Palancar, M. C.; Aragon, J. M.; Torrecilla, J. S. pH-Control System Based on Artificial
26 Neural Networks. *Ind. Eng. Chem. Res.* **1998**, *37*, 2729-2740.
27
28
29
30
31
32
33
34
35
36
37
38
39
40
41
42
43
44
45
46
47
48
49
50
51
52
53
54
55
56
57
58
59
60

ToC Graphics:

